Destabilisation of hydrogen bonding and the phase stability of aniline at high pressure

Post-print of a peer-reviewed article published by the Royal Society of Chemistry.
Published article available at: http://dx.doi.org/10.1039/C2CE26403J

Cite as:
Funnell, N. P., Dawson, A., Marshall, W. G., & Parsons, S. (2013). Destabilisation of hydrogen bonding and the phase stability of aniline at high pressure. *CrystEngComm*, 15(6), 1047-1060.

Manuscript received: 30/08/2012; Accepted: 20/09/2012; Article published: 24/09/2012

Destabilisation of Hydrogen Bonding and the Phase Stability of Aniline at High Pressure**

Nicholas P. Funnell,[1,2] Alice Dawson,[1,3] William G. Marshall[4] and Simon Parsons[1,*]

[1]EaStCHEM, School of Chemistry, Joseph Black Building, University of Edinburgh, West Mains Road, Edinburgh, EH9 3JJ, UK.

[2]Present address: Inorganic Chemistry Laboratory, University of Oxford, South Parks Road, Oxford, OX1 3QR, UK.

[3]Present address: College of Life Sciences, University of Dundee, Dundee, DD1 5EH, UK.

[4]ISIS Pulsed Neutron and Muon Facility, STFC Rutherford Appleton Laboratory, Harwell Science and Innovation Campus, Harwell Oxford, Didcot, OX11 0QX, UK.

[*]Corresponding author; S.P. tel: +44-(0)131 650 4806, fax: +44-(0)131 650 4743, e-mail: s.parsons@ed.ac.uk

[**]We thank The University of Edinburgh and EPSRC for funding and STFC for provision of neutron beam time. We also thank Dr Alan Coelho for advice on restraints in Topas Academic and Mr Andrew Chamberlain (ISIS) for technical assistance during our neutron beamtime.

Supporting information:
†Electronic supplementary information (ESI) available. CCDC 893032–893037. For ESI and crystallographic data in CIF or other electronic format see http://dx.doi.org/10.1039/C2CE26403J

Graphical abstract:

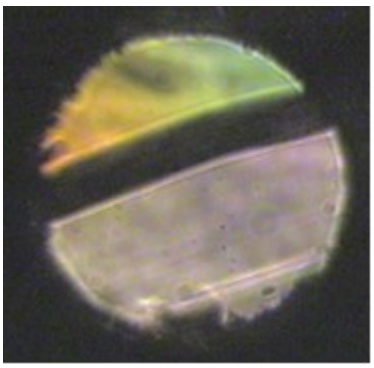

The image shows a crystal of a new phase of aniline growing at a pressure of 8000 atm (0.8 GPa). Hydrogen bonds in this phase become destabilising at 7.3 GPa.

Abstract

Two crystalline phases of aniline have been investigated by a combination of single crystal X-ray diffraction data on aniline-h_7 and neutron powder diffraction data on aniline-d_7. Phase-I, which is formed on cooling the liquid at ambient pressure, is monoclinic ($P2_1/c$). Orthorhombic ($Pna2_1$) phase-II was crystallised at 0.84 GPa at room temperature and structurally characterised at pressures up to 7.3 GPa. The strongest intermolecular interactions in both structures are NH…π contacts and NH…N H-bonds. These interactions occur within layers in both phases, and the phases differ in the way the layers are stacked. The structures of both phases have been obtained under two sets of identical conditions, at 0.84 GPa and 0.35 GPa and studied at room temperature by neutron powder and X-ray single-crystal diffraction. At 0.84 GPa phase-II is the thermodynamically stable form because it has a lower molar volume than phase-I, but as the pressure is reduced the volume of phase-I becomes less than that of phase-II, and at 0.35 GPa phase-II partially transformed into phase-I. PIXEL calculations indicate that the intermolecular interaction energy for pairs of molecules connected by H-bonds is -9 to -16 kJ mol^{-1} in phases I and II at 0.84 GPa, but one of these becomes destabilising in phase-II at 7.3 GPa, with an energy of +1 kJ mol^{-1}, making it similar to several compressed CH…π contacts. The results demonstrate how the hierarchy of intermolecular interaction energies can be manipulated with pressure.

Introduction

In molecular crystals, if the necessary donor and acceptor groups are available, packing is usually directed by hydrogen bonding. Where several H-bonding functionalities are present, it is even possible to quantify the propensity for polymorphism based on different combinations of hydrogen bonds.[1] Hydrogen bonds are, however, quite sensitive to pressure, both in geometry and energy, and the aim of this paper is to explore whether pressure can be used to modify the hierarchy of intermolecular interactions in a crystal structure, changing a hydrogen bond from a highly stabilising interaction into a destabilising one.

The sensitivity of H-bond geometry to pressure can be illustrated by L-alanine, where an intermolecular NH…O H-bond was seen to compress from 1.861(3) Å to 1.69(2) Å at 13.6 GPa.[2] This is the highest pressure for which structural data are available for an organic compound of any complexity, but even at this pressure the NH…O distance is not without precedent at 1 atm. In fact this is more generally the case in compressed structures: 'super-short' H-bonds have not been observed in organic crystal structures at least up to about 10 GPa. In early work this was taken to imply that as an H-bond is compressed the intermolecular interaction in question is driven into a repulsive region of its potential, and that as this point is approached the structure transforms to a different phase where the built-up strain is alleviated.

While relief of strain is a neat paradigm for explaining high pressure transitions in organic solids, when PIXEL packing energy calculations[3-6] were carried out on compressed structures it soon became evident that the situation is more complicated.[7-11] In some cases, such as the phase transition from salicylaldoxime-I to II at 5 GPa,[9] the calculations supported the relief-of-strain model. In most other cases they did not, with some H-bonds, e.g. those in serine,[10] actually becoming *more* stable as they were compressed. In these cases, the need to pack space efficiently, and minimise free energy via the pressure x volume ($p\Delta V$) term, was identified as the driving force for the phase transitions.

Phase stability is determined by free energy, of which internal intermolecular bond energies form just one component. Lattice energies may become smaller in magnitude after a transition provided the other terms, $p\Delta V$ and $T\Delta S$, make up the difference. The serine-I to II phase transition[10] and the formation of salicylamide-II at 0.2 GPa[8] are two examples where this has been demonstrated. Clearly, kinetic factors are also important: in order for one phase to transform to another there has to be a suitable low energy pathway for the transition to occur. It should therefore be possible to 'trap' an unusually short, possibly repulsive, H-bond in a compressed crystal structure, though this has so far not been demonstrated in the organic solid state.

A suitable system for generating a 'repulsive H-bond' using pressure is one where the H-bonding is quite weak before any compression takes place. The weakest conventional H-bonds are those where the H-bond acceptor and donor atoms are both nitrogen. The NH…N hydrogen bond energy in ammonia, for example, has been estimated to be around 10 kJ mol^{-1},[12] which compares to OH…O energies of 20-40 kJ mol^{-1} in phenols and carboxylic acids.[6] The amines are therefore ideal systems to control the extent of stabilisation provided by H-bonding, and in this paper we report the effects of pressure on the crystal structure of aniline (Ph-NH_2).

In addition to reporting crystal structures of aniline at high pressure, we will attempt to quantify the thermodynamic factors responsible for the formation of the different crystalline phases identified. When a material is crystallised the phase obtained often depends on the precise conditions employed, and explaining why a specific form is obtained under a given set of conditions is an important problem in crystal engineering. It is also a highly complex question in many practical crystal growth experiments. For example, modelling polymorphism resulting from growth from different solvents is notoriously difficult, depending on nucleation kinetics as well as thermodynamics. Modelling phase formation at high pressure is a more tractable problem because in varying the pressure we vary a well defined thermodynamic variable.

Aniline (mpt. 267 K) is a liquid under normal conditions, and it was crystallised directly from the liquid state directly by application of pressure. Some other recent experiments involving *in situ* pressure-induced crystallisation include pyridine, nitric acid, sulfuric acid monohydrate and 1,2,3-trichloropropane and solutions which include leucine, and hydrates of sodium sulphate.[13-18] One crystal structure of aniline is available on the Cambridge Structural Database (CSD, Refcode: BAZGOY).[19] The crystal was grown at 252 K, crystallising in the monoclinic space group $P2_1/c$ with the cell dimensions a=21.822(8) Å, b=5.867(4) Å,

c=8.386(6) Å, β=101.01(5)° and *Z*=8 (hereafter referred to as phase I). Vibrational spectra in the solid and vapour phases have been examined in detail, and the thermodynamic properties of aniline have been explored by Takagi, measuring the ultrasonic velocity as a function of pressure and temperature.[20-22] The freezing pressure at ambient temperature is reported in the last of these investigations as being 0.19 GPa. The melting curve of aniline was determined up to 1.2 GPa by Bridgeman in 1914.[23]

Experimental

Sample preparation

High-pressure and low-temperature, single-crystal X-ray diffraction measurements were carried out using aniline-h_7 obtained from Sigma-Aldrich. Neutron powder diffraction measurements were carried out using aniline-d_7 obtained from CDN isotopes. Both samples were used as supplied.

Single-crystal X-ray diffraction study at ambient pressure and 100 K

A sealed glass capillary (o.d. 0.12 mm) containing aniline-h_7 was mounted on a Bruker three-circle Apex II diffractometer equipped with an Oxford Cryosystems low-temperature device. The sample was first super-cooled to 257 K, 10 K below the melting point, and then flash-frozen with liquid nitrogen to yield a polycrystalline mass. An OHCD Laser Assisted Crystal Growth Device was then used to obtain a single crystal using Boese's zone-melting method.[24] Data collections were carried out at 100 K using Mo-Kα radiation. The data were integrated with SAINT and corrected for absorption using SADABS.[25, 26] The structure was solved using direct methods (SIR92).[27] Refinements were performed against F^2 in CRYSTALS.[28] Hydrogen atoms attached to carbon were placed in ideal positions after each cycle of refinement. Hydrogen atoms forming the amino group were refined subject to similarity restraints placed on the N-H distances and HNH and CNH angles. Towards the end of refinement, twinning via a two-fold rotation about the [001] direction was detected using the ROTAX procedure.[29] The twin law, expressed as a matrix, is

$$\begin{pmatrix} -1 & 0 & -1 \\ 0 & -1 & 0 \\ 0 & 0 & 1 \end{pmatrix}$$

and the twin scale factor refined to 0.0135(8). Though the scale is very close to zero, inclusion of twinning in the model reduced R_1(all data) from 5.1 to 4.6%, and so twinning was retained in the final model. Structure

solution and refinement indicated that the sample had crystallised into the previously known monoclinic phase (CSD refcode BAZGOY), aniline-I. Crystal and refinement data at 100 K are listed in Table 1.

Crystallographic information files (cifs) for this and other structures reported herein are available from the Cambridge Crystallographic Data Centre by quoting codes CCDC893032 – 893037.

Single-crystal X-ray diffraction study at 0.8 GPa and room temperature

Aniline-h_7 was loaded into a Merrill-Bassett diamond anvil cell (opening angle 80°), equipped with Boehler-Almax cut diamonds with 600 μm cutlets, a tungsten gasket and tungsten carbide backing plates.[30, 31] A ruby chip was also loaded in the sample chamber so that the pressure could be measured using the ruby fluorescence method.[32] The pressure was slowly increased while monitoring the appearance of the sample with a polarising microscope. Crystallisation to a polycrystalline mass occurred at 0.8 GPa. The cell was then heated until only one crystallite remained. The cell was then allowed to cool slowly, causing the crystal to grow until it filled the sample chamber (*ca.* 0.3 x 0.3 x 0.05 mm). Images of the crystal growth starting from a single crystallite are shown in Figure 1a.

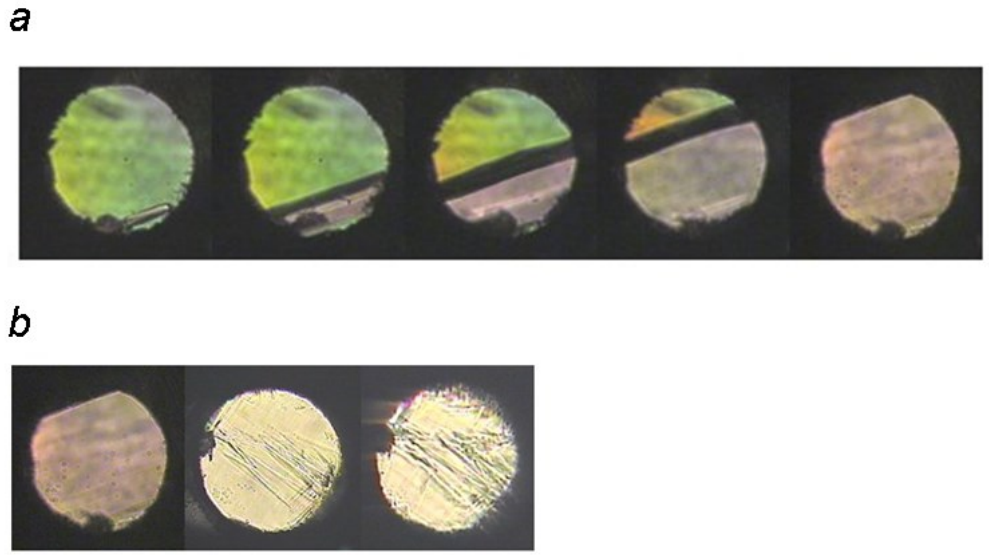

Figure 1. (*a*) Crystal growth of aniline-II at 0.8 GPa. The diameter of the circular sample chamber is 0.3 mm. The apparent colouration of the crystal and liquid phases is due to the use of a polariser. (*b*) Images of the crystal of aniline-II at 0.8 GPa (left), 0.5 GPa (centre) and 0.3 GPa (right). The crystal surface becomes increasingly cracked as pressure is decreased. The dark object at the edge of the cell chamber is the ruby chip used for pressure measurement.

X-ray diffraction data were collected with Mo-Kα radiation on an Agilent Technologies SuperNova diffractometer. Data were integrated and corrected for absorption using CrysAlisPro[33] then merged with SORTAV.[34] Data collections were carried out at room-temperature and a pressure of 0.8 GPa and then at 0.7, 0.5 and 0.3 GPa. Structure solution and refinement indicated that the sample had crystallised into a previously unknown orthorhombic phase, hereafter designated 'aniline-II'. The data were used in the 'XN' refinement against both X-ray and neutron diffraction data described below.

High-pressure neutron powder diffraction experiments

Aniline-d_7 was mixed in 4:1 volume ratio with a 4:1 mixture of deuterated methanol and ethanol; the alcohols were included to act as a hydrostatic medium during compression. The mixture was loaded into a TiZr sample gasket along with SiO_2 wool, which provided multiple nucleation sites, and polycrystalline CaF_2 as a pressure marker.[35] Pressure was applied with a V3-type Paris-Edinburgh press equipped with high-transmission zirconia-toughened alumina anvils. Fluorite (CaF_2) was used as a pressure marker because its diffraction peaks suffered from less overlap with those predicted for aniline than other common (and softer) markers such as NaCl or Pb. Pressures were calculated from the refined lattice parameter of CaF_2 using a third-order Murnaghan equation of state with V_0 =163.293 Å^3, K_0 = 81.0 GPa and K' = 5.22.[36]

Neutron powder data were collected using the time-of-flight technique on the PEARL beamline at the ISIS spallation source.[37, 38] Pressure was applied to the sample, which had crystallised into orthorhombic phase-II at 0.71 GPa. Data sets were collected up to 7.3 GPa at intervals of *ca.* 0.3 GPa over the *d*-spacing range $0.6 < d < 4.1$ Å. The patterns at 0.84 and 7.3 GPa are shown in Figures 2 a and b. The sample was then partially decompressed and data were collected at 3.95, 2.34, 1.39, 1.11, 0.95 and 0.60 GPa. Throughout this pressure series the sample remained in phase-II. On reducing the pressure to 0.35 GPa the sample became a mixture of phases I and II (Figure 2c). On further decompression to 0.31 GPa the aniline pattern disappeared, as the sample melted or redissolved in the hydrostatic medium. The sample was then re-crystallised by increasing the pressure back up to 0.65 GPa. This formed phase I. Further compression data were then collected at 0.57, 0.84 (Figure 2d) and 1.04 GPa.

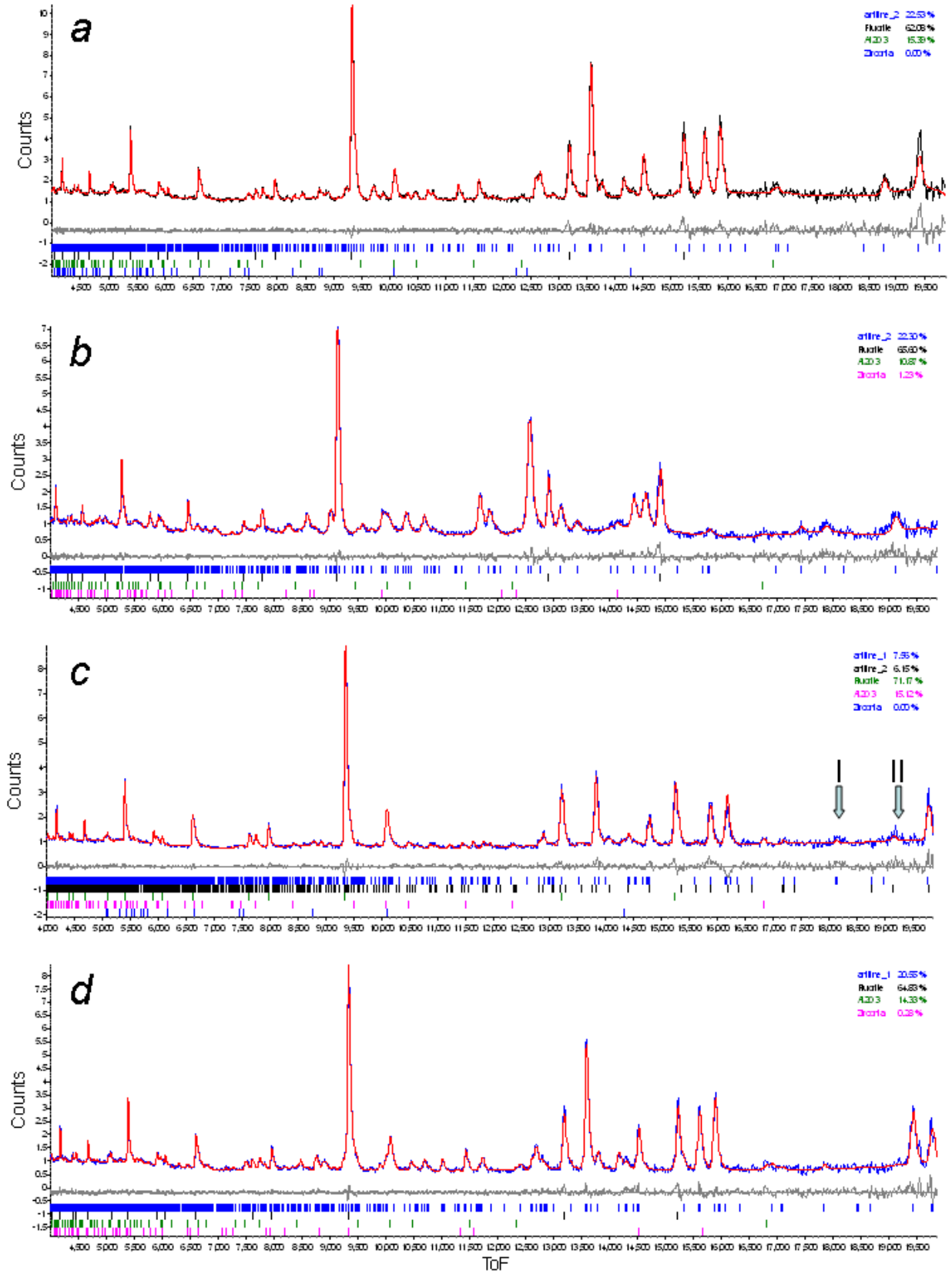

Figure 2. Rietveld fits to neutron powder diffraction data. (a) Aniline-II at 0.84 GPa and (b) 7.3 GPa; (c) Mixture of aniline-I and II after decompression of phase II to 0.35 GPa. The arrows marked I and II indicate diagnostic peaks for these phases. (d) Phase-I at 0.84 GPa.

'XN' Refinement of Phase II at 0.84 GPa

Diffraction data for phase II were available at 0.8 GPa from the single crystal X-ray diffraction experiment and at 0.84 GPa from the neutron powder diffraction experiment; the cell volumes were 976.86(18) and 973.06(15) $Å^3$, respectively. The crystal structure of aniline-II was jointly refined against both data sets using the program TOPAS Academic version 5.[39] The refinement model consisted of a Z-matrix description of the aniline molecules where the C_6H_5N moiety was constrained to have mirror symmetry with respect to the N…C_{para} axis; distances and angles within this fragment were constrained to be equal for both molecules in the asymmetric unit. Separate parameters were assigned to the four H-N1-C1-C2/6 torsion angles involving the amine groups; the N-atoms were also allowed to move out of the plane of the phenyl ring, but the phenyl rings were constrained to be planar. All C-H and N-H bond distances were respectively constrained to be equal. A parameter representing the difference between bond distances involving H in X-ray and D in neutron models refined to 0.099(9) Å. The position and orientation of the molecules were assumed to be the same for both data sets. For the X-ray model all non-H atoms were refined with anisotropic displacement parameters and a common isotropic displacement parameter was refined for the H-atoms. For the neutron data, common isotropic displacement parameters were refined for the non-D atoms in each of the two molecules, the displacement parameters of the D-atoms were set equal to 1.2 x or 1.5 x the displacement parameter of the parent C or N atom. The weighting schemes applied to the X-ray and neutron data sets were respectively scaled by 0.944 and 1.850 so that each data set yielded a goodness of fit near unity.

Also included in the neutron powder pattern models were CaF_2 (the pressure marker) and Al_2O_3 and t-ZrO_2 (components of the Paris-Edinburgh cell anvil cores).

The refinement model of aniline at this stage was used to validate periodic DFT structure optimisations using the BLYP exchange-correlation functional (see below). For consistency with the other refinements reported here, in the final stages of refinement restraints (described below) derived from the DFT calculations were also applied to the XN refinement. This increased the weighted residual factor from 11.4 to 11.7% for the X-ray data set and 4.126 to 4.137% for the neutron data set. Final crystal and refinement data at 0.84 GPa are listed in Table 1.

Refinements Against Neutron Powder Diffraction Data

Neutron powder diffraction data are available for phase-I at 0.84 GPa and phase-II at 7.3 GPa. The parameters used to define the refinement models were the same as described for the XN refinement above. In the initial stages of Rietveld refinement only the unit cell dimensions and the molecular positional and orientation parameters were refined. This approximate model was then optimised by periodic DFT using the BLYP functional. The DFT-optimised parameters were then incorporated into the Rietveld refinement as restraints

(see below), and all parameters, including internal bond distances, angles and torsions and molecular position and orientation parameters, were allowed to refine.

Data are also available from the mixture of phases I and II obtained at 0.35 GPa on decompression of phase-II from 7.3 GPa. These data were modelled in the same way as described for the other data sets except that the structural, positional and orientation parameters were held fixed at the values obtained at 0.84 GPa to reduce the number of parameters being refined.

Crystal and refinement data for all refinements are listed in Table 1.

Phase	I	I	II	II	II	I	II
Pressure/ GPa	0	0.84	0.84	0.8	7.3	0.35	
Temp-erature/K	100	298	298	298	298	298	
Radiation	X-ray[b]	Neutron[c]	Neutron[a,c]	X-ray[a,b]	Neutron[c]	Neutron[c]	
Space group	$P2_1/c$	$P2_1/c$	$Pna2_1$	$Pna2_1$	$Pna2_1$	$P2_1/c$	$Pna2_1$
a, *b*, *c* Å/	21.5674(8) 5.8052(2) 8.2949(3)	21.3572 (18) 5.6983(6) 8.1808 (5)	8.1682(6) 5.6885(6) 20.9418(19)	8.1757(14) 5.6902(3) 20.9980(9)	7.5195(8) 5.2737(9) 19.578(2)	21.721(7) 5.7889(12) 8.3229(12)	8.3307(15) 5.8167(17) 21.275(7)
β/°	101.043(2)	100.973(12)	90	90	90	101.10(4)	90
V /Å^3	1019.32(6)	977.41 (15)	973.06(15)	976.86(18)	776.36(17)	1027.0(4)	1030.9(5)
Z	8	8	8	8	8	8	8
R_{int} or R_{Pawley}[d]	0.043	0.031	0.031	0.049	0.035	0.043	
R, S[e]	0.039, 0.098, 1.00	0.046 0.81	Neutron: 0.041, 1.00 X-ray: 0.053, 0.117, 1.00 All: 0.045, 1.00		0.041 0.73	0.059, 0.06	
No. indep-endent obs-ervations[f]	1796	2675	2675	692	2675	2675	
Parameters	144	75	196		73	51	
Restraints	10	28	27		27	0	

[a]. XN Refinement. [b]. Single crystal refinement against X-ray data. [c]. Rietveld refinement against powder data. [d]. R_{int} quoted for single crystal data sets, R_{wp} for a Pawley refinement is quoted for the Rietveld refinements. [e]. For single crystal $R[F^2 > 2\sigma(F^2)]$, $wR(F^2)$, S, for powder data R_{wp} and S. The weighting scheme for the mixed-phase refinement at 0.35 GPa was $w = 1/I_{obs}$ which led to better fitting of the low d-spacing data where differences between phases I and II are greatest and lower standard deviations for the cell parameters. For other refinements $w = 1/\sigma^2(I_{obs})$. [f]. For single crystal data the number of independent reflections, for powder data the number of data points.

Table 1. Crystal and refinement data for aniline-I and -II at different pressures.

In order to obtain an overview of the path of compression of phase-II, all neutron powder data sets were modelled together in a single refinement. Distance, angle and torsion parameters were held fixed to those obtained in the XN refinement at 0.84 GPa. The positions and orientations of the molecules were refined subject to DFT-derived restraints. Isotropic displacement parameters were set equal to the parametric equation $B_0 + B_1$ x Pressure where B_0 and B_1 were allowed to refine. The result is available in Quicktime movie format in the supplementary material.

DFT calculations

Geometry optimisations were performed by periodic Density Functional Theory (DFT) using the DMOL^3 code[40] as part of the Materials Studio modelling suite.[41] The DNP numerical basis set[42] was used in combination with the BLYP functional.[43, 44] The unit cell dimensions were held fixed at the values obtained in the Rietveld refinements of the neutron powder diffraction data described above, and coordinates were allowed to optimise. Convergence was defined when the maximum changes in total energy, displacement and gradient were 10^{-5} Ha, 5 x 10^{-3} Å and 2 x 10^{-3} Ha Å^{-1}, respectively. Brillouin zone integrations were performed by Monkhorst-Pack[45] k-point sampling at intervals of 0.07 Å^{-1}. Vibrational frequencies were calculated at the Γ-point only; all calculated frequencies were real.

The DFT-optimised structures were used to formulate restraints which were then applied to the Rietveld refinements. In order to ensure that these restraints were consistent with the refinement constraints (e.g. mirror symmetry, planar phenyl rings etc), ideal single crystal X-ray diffraction data were calculated (XPREP)[46] from the DFT-optimised structures and the constrained model refined against these 'data'. The bond distance, angle, torsion, position and orientation parameters of the Rietveld refinements were restrained to the values obtained. The 'esds' applied to the restraints, which determine their weights, were 0.01 Å for bond distances, 1° for bond angles, 2° for torsions, 0.01 for fractional coordinates and 2° for the rotational angles used to code for molecular orientation.

PIXEL calculations

The molecular electron densities in the crystal structures of phase I at 100 K and 0.84 GPa and phase II at 0.84 and 7.3 GPa at room temperature were calculated using the program GAUSSIAN09[47] with the MP2/6-31G** basis set. The electron density was used to evaluate packing energies using the PIXEL method[3-5] as implemented in the program OPiX.[48]

Other programs used

Searches of the Cambridge Structural Database (CSD) used ConQuest v1.14, with database updates up to May 2012.[49, 50] Crystal structures were visualised using Mercury CSD 2.3[51] and Diamond.[52] INS spectra were visualised with ACLIMAX;[53] the experimental INS spectrum of aniline was taken from the database available via the TOSCA instrument website at the ISIS facility (http://www.isis.stfc.ac.uk/instruments/tosca/ins-database/ins-database9060.html). The bulk modulus of aniline-II was calculated using EOSFIT.[54] Geometric calculations were accomplished in PLATON.[55] Hirshfeld surface calculations were carried out with CrystalExplorer version 3.[56]

Results

Phase I

Aniline-I is was obtained by cooling the liquid at ambient pressure, and its structure was determined from a twinned crystal using X-ray diffraction at 100 K. The structure of this phase at 252 K has been previously reported by Fukuyo *et al.* (CSD refcode BAZGOY).[19] It is monoclinic ($P2_1/c$) with two molecules in the asymmetric unit. The numbering scheme for one of the molecules (#1) in the asymmetric unit is shown in Figure 3a: molecule #1 consists of atoms N11, C11, C21 *etc.,* while molecule #2 conatins N12, C12, C22 *etc.* The two molecules of the asymmetric unit are related by a non-crystallographic rotation of approximately 180° (-176.6°) about the *c* direction ([0.00 -0.03 -1.00]). This is the same relationship as is expressed in the twinning.

Intramolecular bond distances and angles adopt values located near the centres of distributions for similar moieties harvested from the CSD (MOGUL).[57] Though aniline is approximately planar, the N-atom is displaced from the plane of the aromatic ring by 0.117(1) and 0.108(1) Å in the two independent molecules at 100 K (Figure 3b). The deviations obtained in the periodic DFT optimisations were 0.144 and 0.150 Å, and the effect has also been noted in optimisations of the isolated aniline molecule (deviation *ca*. 0.1 Å depending on the basis set and level of theory).[22] The angles made by the NH_2 planes with those of their respective phenyl groups are 33.6(11) and 34.7(11)°. There is also a small twist about the N-C bond, and the difference ($\Delta\tau$) between the magnitudes of the H111-N11-C11-C21 and the H112-N11-C11-C61 torsion angles is 5.8(1)°; the corresponding figure for molecule #2 is 11.0(1)°.

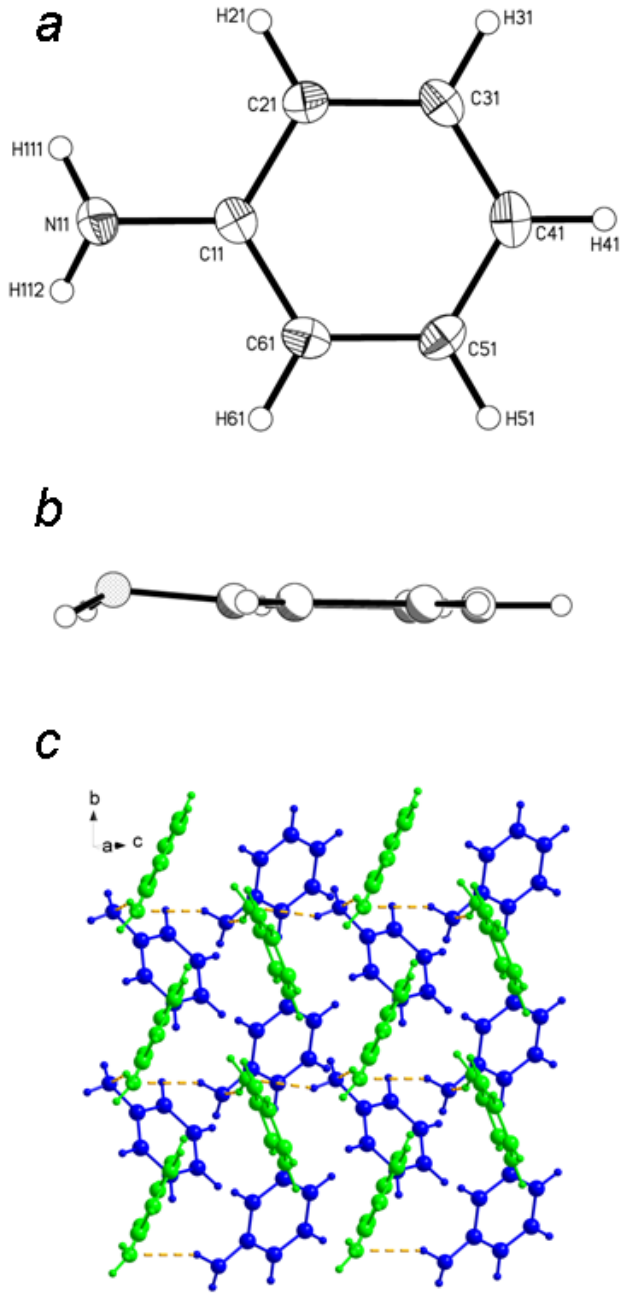

Figure 3. Aniline-I at 100 K. (a) The structure of one of the molecules (#1) in the asymmetric unit. Ellipsoids enclose 50% probability surfaces. (b) The same molecule as in (a) viewed side-on to show the deviation of the amino group from the phenyl plane. (c) View of one layer viewed approximately along **a*** showing CH…π and π…π interactions. Molecules #1 and #2 are shown in green and blue.

Although H-bonds are present (see below),[158] PIXEL calculations show that the strongest intermolecular interactions are NH…π contacts in which molecules related by *c*-glides build-up chains (Figure 4a, Table 2). The molecule…molecule energies of these interactions calculated by the PIXEL method are both around -21 kJ mol^{-1}. The NH…π chains are connected by NH…N hydrogen bonds formed between N11-H112…N12 and N12-H122…N11 in which the (normalised) H…N distances are 2.24 and 2.39 Å, respectively, with molecule-molecule energies of -12.8 and -15.2 kJ mol^{-1}. Other geometric parameters are given in Table 2.

The combination of the NH…π contacts and NH…N H-bonds build double chains which run along **c** (Figure 4a). Lattice repeats along **b** generate layers in which the phenyl groups of neighbouring chains interact via CH…π (8 kJ mol^{-1}) and off-set stacking (12 kJ mol^{-1}) interactions (Table 2, Figure 3c). The layers are stacked along **a**, and a molecule in one layer interacts with a symmetry equivalent of itself generated by inversion centres or 2_1 screw axes in the layer above. H31 and H32 are directed into a groove on the surface of the layers above and below making dispersion-dominated interactions with three molecules with energies in the range 6-8 kJ mol^{-1}.

Phase/Conditions	I at 100 K	I at 0.84 GPa	II at 0.84 GPa	II at 7.3 GPa
Chain-Building Interactions				
N11-H111...π to Cg1^{i}				
Distance/Å	2.52	2.51(4)	2.468(14)	2.15(3)
<N-H…Cg/°	149	153(3)	147.0(11)	136(3)
Energy/ kJ mol^{-1}	-21.1	-21.4	-21.6	-15.9
N12-H121...π to Cg2^{ii}				
Distance/Å	2.51	2.52(3)	2.435(15)	2.19(3)
<N-H…Cg/°	140	141(3)	144.6(11)	137(3)
Energy/ kJ mol^{-1}	-21.3	-21.4	-22.4	-18.4
N11-H112 ..N12^{iii}				
Distance H...N/Å	2.24	2.12(5)	2.195(15)	1.90(4)
Distance N...N/Å	3.1729(19)	3.00(5)	3.117(10)	2.85(3)
<N-H…N/°	151	142(4)	149.7(10)	154(3)
Energy/ kJ mol^{-1}	-12.8	-9.6	-13.3	+1.1
N12-H122 ..N11^{iv}				
Distance H...N/Å	2.39	2.31(5)	2.357(15)	2.13(4)
Distance N...N/Å	3.3215(19)	3.26(4)	3.279(10)	3.06(4)
<N-H…N/°	151	152(4)	149.6(10)	154(3)
Energy/ kJ mol^{-1}	-15.2	-15.9	-13.6	-10.9
Layer-Building Interactions				
C41-H41...Cg1^{v}				
Cg...Cg/ Å	4.7937(9)	4.721(10)	4.709(3)	4.339(8)
H…Cg/Å	3.09	3.099(17)	3.045(4)	2.633(11)
<C-H…Cg/°	118	114.7(14)	116.6(2)	116.4(5)
Energy/kJ mol^{-1}	-8.1	-6.9	-7.2	+6.6

[1] H-atom positions determined by X-ray diffraction have been adjusted by 'normalising' C-H or N-H distances to typical neutron values, C-H = 1.089 Å and N-H = 1.015 Å.

C42-H42...Cg2[vi]				
Cg...Cg/ Å	4.9233(9)	4.791(9)	4.799(3)	4.362(8)
H…Cg/Å	3.22	3.155(16)	3.138(4)	2.729(12)
<C-H…Cg/°	119	115.4(14)	116.9(3)	114.0(9)
Energy/kJ mol^{-1}	-7.8	-7.7	-7.9	-0.2
C61-H61...Cg2[vii]				
Cg...Cg/ Å	6.4355(9)	6.394(13)	6.359(2)	5.969(7)
H…Cg/Å	3.99	3.96(4)	3.918(10)	3.56(2)
<C-H…Cg/°	170	175(2)	170.2(7)	169.2(18)
Energy/kJ mol^{-1}	-5.8	-6.5	-6.2	-5.6
Cg1/2...Cg1/2[viii]				
Cg…Cg/Å (= *b*)	5.8052(10)	5.698(11)	5.688(2)	5.273(8)
Energy/kJ mol^{-1}	-11.6/-12.1	-11.6/-13.2	-12.2/-12.2	-5.4/-5.3
Stacking Interactions				
C31-H31..Cg1[ix]			**C31-H31..Cg2[ix]**	
Cg…Cg/Å	5.7773(9)	5.728(13)	5.751(2)	5.260(7)
H…Cg	3.67	3.52(3)	3.649(10)	3.20(2)
<C-H…Cg	140	147.4(16)	140.6(5)	139.3(13)
Energy/kJ mol^{-1}	-7.2	-7.9	-7.6	-1.3
Cg1…Cg1[x]			**Cg1...Cg2[x]**	
Cg…Cg/Å	6.4027(9)	6.332(13)	6.275(3)	5.879(7)
Energy/kJ mol^{-1}	-6.0	-6.2	-6.4	-4.8
C32-H32…Cg2[xi]			**C32-H32…Cg1[xi]**	
Cg…Cg/Å	5.8314(9)	5.632(12)	5.663(2)	5.236(7)
H…Cg	3.72	3.52(3)	3.538(10)	3.14(2)
<C-H…Cg	140	141.3(15)	141.8(5)	141.3(14)
Energy/kJ mol^{-1}	-7.2	-7.4	-7.3	-1.8
Cg2…Cg2[xii]			**Cg2...Cg1[xii]**	
Cg…Cg/Å	6.3795(9)	6.162(10)	6.275(3)	5.879(7)
Energy/kJ mol^{-1}	-6.3	-6.6	-6.4	-4.8

	Operation in phase I	Operation in Phase 2
i	x 0.5-y -0.5+z	-0.5+x 0.5-y z
ii	x 0.5-y -0.5+z	0.5+x 1.5-y z
iii	x 0.5-y 0.5+z	0.5-x -0.5+y 0.5+z
iv	x y -1+z	1-x 1-y -0.5+z
v	x 1.5-y 0.5+z	0.5+x 1.5-y z
vi	x 1.5-y 0.5+z	0.5+x 0.5-y z
vii	x 1.5-y 0.5+z	0.5-x 0.5+y 0.5+z
viii	x -1+y z	x, -1+y, z
ix	1-x -0.5+y 1.5-z	0.5+x 0.5-y z
x	1-x 1-y 2-z	1+x y z
xi	2-x -0.5+y 0.5-z	-0.5+x 1.5-y z
xii	2-x 1-y 1-z	-1+x y z

Table 2. Intermolecular Interactions and energies for aniline. Cg1 indicates the centroid of the phenyl ring of molecule #1. All values were calculated in PLATON. H-atom positions determined by X-ray diffraction have been normalised as described in the text.

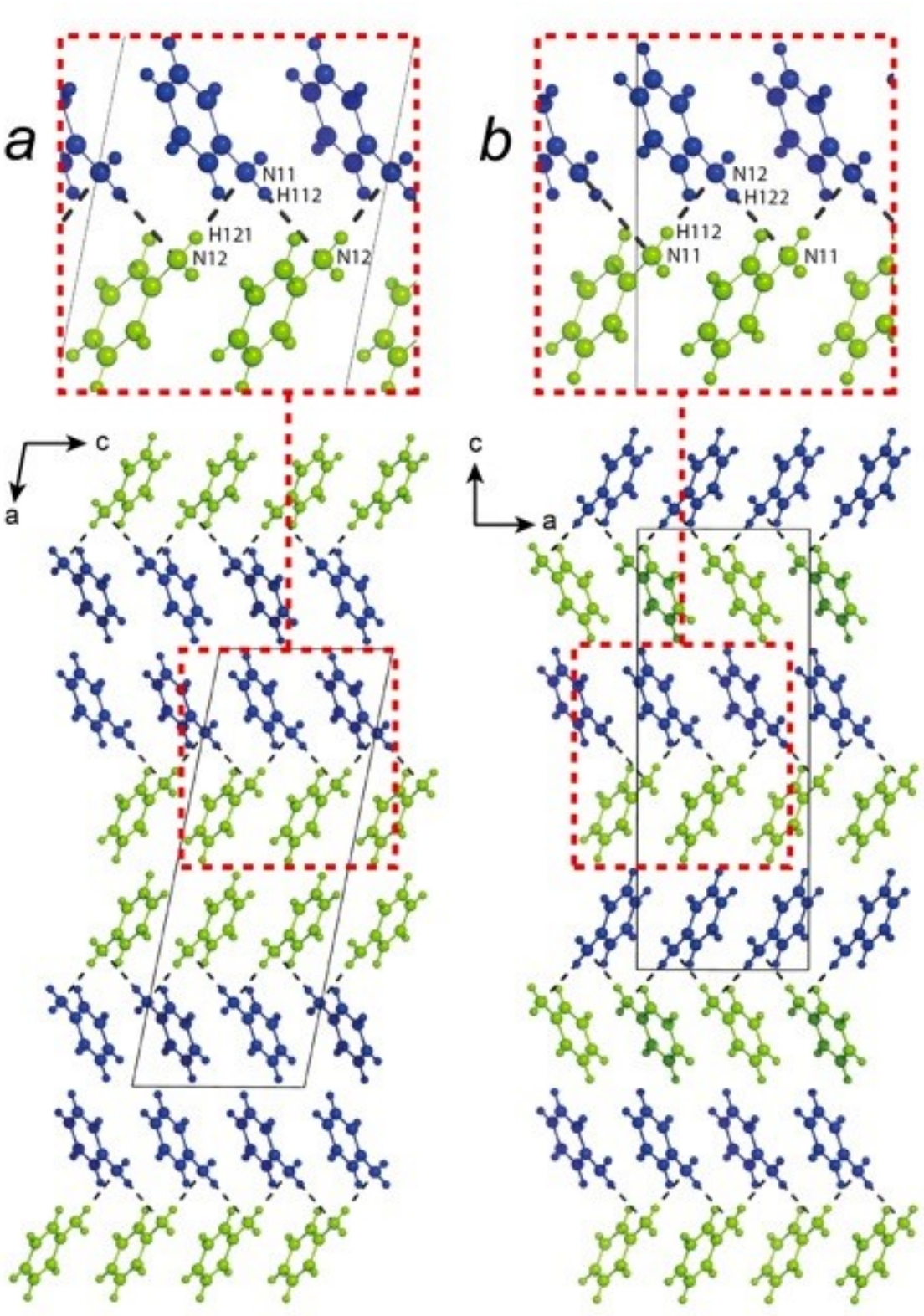

Figure 4. Crystal structures of (a) phase I at 150 K and (b) phase II at 0.8 GPa (left). Both views are projected along the *b*-axis. Molecules are coloured by symmetry equivalence.

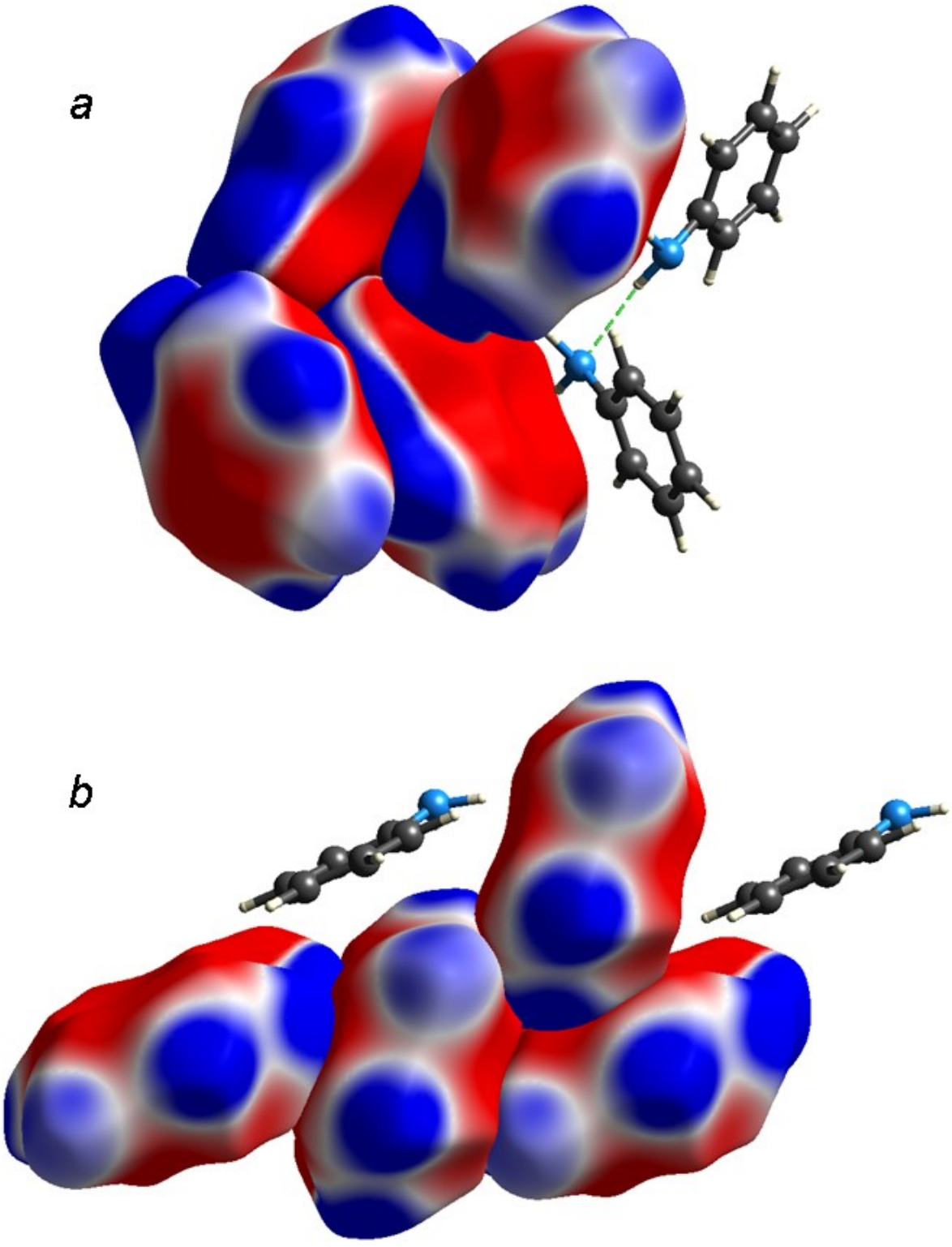

Figure 5. Hirshfeld surfaces in Aniline-I at 0.84 GPa coloured according to electrostatic potential covering the range ±0.01 au. The STO-3G basis set was used for the calculations. Negative regions are red, positive regions blue. (a) NH…N and NH…π contacts in the layes. (b) One layer viewed from above (*cf*. Figure 3c) showing off-set stacking (vertical) and CH…π contacts (horizontal). Note the alignment of the white zero-potential regions where the molecules in the centre of part b interact by an off-set stacking contact.

Hirshfeld surfaces[59, 60] coloured according to electrostatic potential[61] (Figure 5) illustrate the electrostatic complementarity of the interactions described above. The strength of the NH…π contacts (running horizontally in Figure 5a) correlates with the large red (negative) and blue (positive) area in contact. The long off-set distances in the stacking contacts within the layers (running vertically in Figure 5b) correspond to alignment of the white zero electrostatic potential regions in the contacting molecules.

The structure of phase I has been determined at ambient pressure and 100 K and at 0.84 GPa and ambient temperature. Direct comparison is complicated by opposing thermal and pressure effects, but the respective unit cell volumes, 1019.32(6) and 977.41(15) Å^3, show that pressure effects dominate. The *a*, *b* and *c* axis lengths decrease by 0.98, 1.83 and 1.37%, respectively, and the largest eigenvalue of the strain tensor also lies along *b*. The volume is reduced by compressing the off-set stacking and CH…π interactions that link the H-bonded chains into layers, notably the CH…π interactions involving H41 and H42 (Table 2, Figure 3c). Intermolecular interaction energies are similar to those at 100 K. There was no statistically significant difference in the conformation or orientation of the amino group to that observed at 100 K.

Phase II

Aniline crystallises into phase-II on compression of the liquid to 0.8 GPa, though a sample of phase-II remains as a solid down to pressures to *ca* 0.3 GPa, and the higher crystallisation pressure may be the pressure equivalent of super-cooling.

The structure of phase-II at 0.84 GPa was determined in a joint refinement against X-ray single crystal data on aniline-h_7 and neutron powder data on aniline-d_7. The space group is $Pna2_1$, and, like phase I, the structure contains two molecules in the asymmetric unit. The orientations of the molecules are related by an approximate two-fold axis (rotation angle = -178.5°) about a direction close to **a** ([-1.000 0.010 0.006]), the same direction as in phase-I (i.e. along the 8 Å unit cell axis).

The deviations of the N-atoms from the planes of the phenyl groups [0.123(8) and 0.124(8) Å] are similar to those in phase-I. Neither are there any significant differences in the conformation of the amino group. For molecule #1 the angle between the amino and phenyl planes is 33.5(12)° with $\Delta\tau$ = 8.1(18)°. For molecule #2 the corresponding values are 39.0(12)° and 13.2(19)°.

Intermolecular interactions in phase-II are very similar to those in phase-I. In phase-I the strongest interactions are those formed within the strands of molecules connected by NH…π and NH…N H-bonds. The next strongest interactions are the offset stacking and CH…π contacts which connect the strands into layers. The same comments are true in phase-II, and individual layers in the two phases are super-imposable on one another, with similar interaction distances and energies between the molecules (Table 2). The weakest

interactions in phase-I are those mediating the stacking of the layers, and the phases differ in the way that the layers are stacked.

Phase II is not very different to phase-I. Direct comparison of the cell dimensions can be misleading because whereas II is orthorhombic, I is monoclinic with β ~101°.; *d*-spacings between equivalent sets of principal planes [*e.g.* (100) in I and (001) in II] are a better guide, and these are in I/II (Å): 20.97/20.94, 5.70/5.69 and 8.03/8.17. One method for measuring the similarity between two crystal structures available in MERCURY is to calculate the correlation coefficient between their X-ray powder patterns. A value of 1.0 indicates a perfect match; the value for aniline I and II at 0.84 GPa is 0.99. The similarity also extends to the neutron powder patterns, which with the exception of a few peaks between 3 and 4 Å are virtually super-imposable.

Figure 6 shows the relationship between the structures of the two phases. The diagram is available in the form of as an animated gif (Phase_I_II_animation.gif) in the Supplementary Material. At the bottom of the figure the layers, composed of the rows labelled 'row 1' and 'row 2', from the two phases are superimposed. The molecules within the layers are related by cell translations (along the 5 Å cell axes) and glide planes. In phase-I neighbouring layers are related by inversion and 2_1 operations of space group $P2_1/c$. In phase-II they are related by the 2_1 screw axes and *n* glides of $Pna2_1$. This means that when the layers stack, in phase-I molecules of type #1 or 2 interact with symmetry equivalents of themselves, whereas in phase-II molecules of type #1 interact with molecules of type #2.

Moving up in Figure 6, the next row ('row 3') of molecules of type #1 in phase-I superimpose well with molecules of type #2 in phase-II. This superposition occurs because of the non-crystallographic symmetry which exists within the asymmetric units of both phases. In phase-II the orientation of molecule #2 is related to that of molecule #1 by a pseudo 2-fold rotation about *a*; when molecule #2 undergoes a 2_1 space group operation along *c*, the combined effect relative to molecule #1 is a near 2-fold operation about *b* (the 8 Å axis in phase-II). This image of molecule #2 therefore superimposes on an image of molecule #1 in phase-I generated by a 2_1 operation along *b* (also the 8 Å axis in phase-I).

In the top row of molecules in Figure 6 ('row 4') images of molecules of type #2 in phase-I generated by inversion or 2_1 operations lie on top of molecules of type #1 in phase-II generated by 2_1 or *n* glides. Pairs of molecules are therefore mirror images of each other and the superposition fails. Superimposition is again attained after four layers (in rows 9 and 10, not shown in Figure 6).

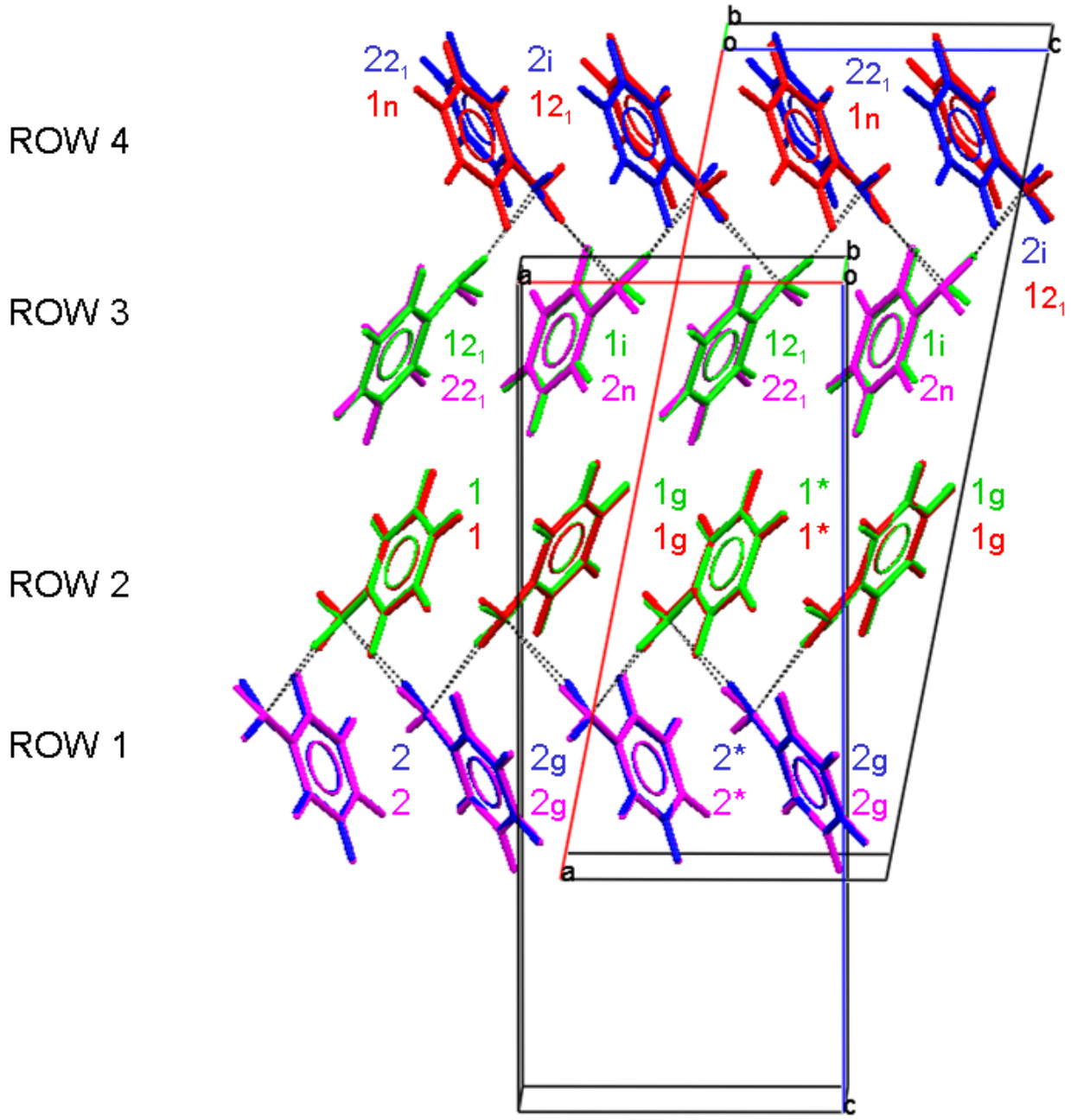

Figure 6. Overlay of phases I and II. Molecules #1 and #2 in the asymmetric unit are coloured green and blue for phase I and red and magenta for phase-II. Symmetry operations are screw axes (2_1), *c* or *a* glides in phases I and II (labelled g), *n* glides in phase II (n) and inversion centres in phase I (i). Molecules in the asymmetric unit are labelled with a *, molecules related to these by lattice translations carry no symmetry label. A blue 2i indicates molecule #2 in phase I related to the asymmetric unit by an inversion operation. Superposition works well for Rows 1, 2 and 3 where both molecules in either phase are related to the asymmetric unit by proper or improper operations. In Row 4 the operations are mixed and the overlay fails. Pairs of rows (1/2 and 3/4) form one 'layer'.

Comparison of the geometric parameters associated with equivalent interactions in phases I and II at 0.84 GPa in Table 2 presents a very consistent picture. Interaction energies are also similar, and the lattice energies (as calculated by PIXEL) of the two phases at 0.84 GPa are virtually identical, -79.2 (I) and -79.8 (II) kJ mol^{-1}. It is thus not possible to point to any specific interaction as being responsible for the relative stability of phase-II at high pressure.

The effect of pressure on Phase-II

The crystal structure of aniline-II at 0.84 GPa is shown in Figure 4b, with the corresponding Rietveld fit in Figure 2a. The effect of pressure on the cell volume is shown in Figure 7. The path of compression can also be visualised in a Quicktime movie included in the supplementary material (Phase2_compression.mov). Between 0.84 and 7.3 GPa the *a*, *b* and *c*-axes compress by 8.3, 7.7 and 6.8% respectively, corresponding to a compression in volume by 21%. As in phase-I, the least compressible direction is the that corresponding to the long unit cell axis (*a* in phase-I, *c* in phase-II). The direction of greatest strain now corresponds to the *b*-axis, the direction of the NH…π and NH…N H-bonds; these contacts decrease by between 10 and 13% (Table 2). The compression in the NH…π contacts has rather little effect on their interaction energies, but the NH…N H-bonds are pushed into a destabilising region of their potential (the energy of N11-H112…N12 is +1.1 kJ mol^{-1}). The centroid-to-centroid distances in the various phenyl group interactions decrease by between 6 and 9%, but some of these also become destabilising, notably the CH…π contacts which build the layers have energies of +6.6 kJ mol^{-1}.

The bulk modulus (K_o) of phase II derived from fitting the volume *versus* pressure data to a Vinet equation of state[62, 63] is 5.39(22) GPa (Figure 7). The values of K' and V_0 refined to 9.11(14) and 1077(3) $Å^3$ respectively. The bulk modulus indicates that aniline is a soft solid, a reflection of the relatively weak intermolecular interactions. The value is actually similar to that of the van der Waals crystal $Ru_3(CO)_{12}$, 6.6 GPa,[64] and rather smaller than for a more strongly H-bonded crystal such as L-alanine [13.1(6) GPa].[2] The projected ambient-pressure volume (V_0) is substantially higher than the phase-I volumes observed experimentally at 252 K (1053.9 $Å^3$) and extrapolated to 300 K (1065 $Å^3$). The suggestion that phase-II has a higher volume than phase-I at low pressures is consistent with the results from refinement of a mixed phase model against data obtained at 0.35 GPa (described in the following section).

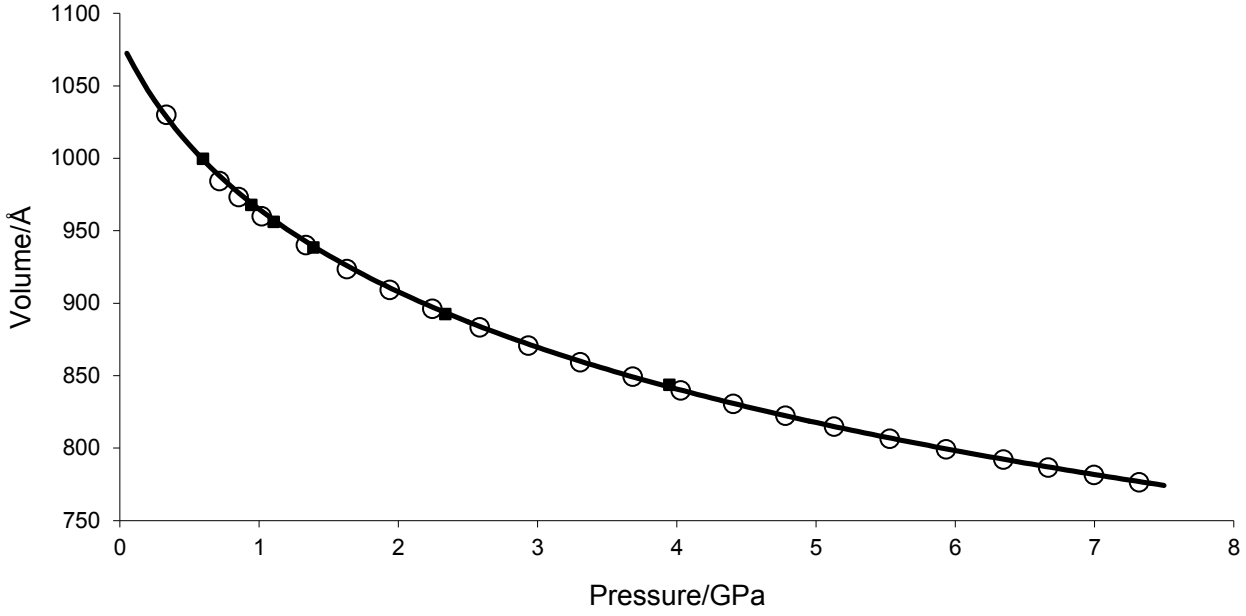

Figure 7. Unit cell volume of phase-II versus pressure. The open circles correspond to increasing pressure, the black squares to decreasing pressure. The line is calculated from the Vinet equation of state (EoS) as described in the text. Only the pressure-increasing points were used to determine the EoS.

Decompression of Phase-II

Following collection of the 0.8 GPa single crystal X-ray data set the sample was carefully decompressed. At 0.8 GPa the cell dimensions of aniline-II are a=8.1757(14) Å, b=5.6902(3) Å and c=20.9980(9) Å. At 0.50 GPa the corresponding values are a=8.205(9) Å, b=5.7371(14) Å and c=21.022(6) Å. The crystal cracked as the pressure was reduced (Figure 1b) and 0.27 GPa was the lowest pressure at which data could be collected. At this pressure, however, the diffraction pattern was of poor quality and could not be indexed.

The behaviour of the powder sample was different. Neutron powder diffraction data collected on decompression showed that the sample remained in phase-II until 0.6 GPa. The cell dimensions on decompression followed the same trend as they did on compression, showing no evidence of hysteresis (Figure 7). The powder pattern obtained at 0.35 GPa shows two weak diagnostic peaks at d = 3.75 and 3.95 Å (indicated with arrows in Figure 2c), indicating that at this pressure the sample had become a mixture of phase I and II. Rietveld refinement indicates that the phases are present in approximately equal quantities. Crystal and refinement data are given in Table 1, but it is notable that the volume of phase-II is slightly *higher* [1030.9(5) Å^3] than that of phase-I [1027.0(4) Å^3]. The failure to observe a similar transition in the single crystal is possibly a kinetic effect, though it could also be because different isotopologues (aniline-h_7 or d_7) were used in the two studies.

Further decompression of the powder sample to 0.3 GPa induced melting or dissolution in the hydrostatic medium. When pressure was reapplied a pattern was obtained at 0.65 GPa corresponding to pure phase-I. The

pattern obtained at this pressure was solely that of phase I, with cell dimensions *a*=21.460(7) Å, *b*=5.7329(5) Å, *c*=8.2274(5) Å and β=100.962(9)°. Further phase I diffraction patterns were then collected at 0.84 (Figure 2d) and 1.04 GPa. The structure derived from the 0.84 GPa data set is described above, but there was no evidence for phase II even at 1.04 GPa.

Validation of theoretical methods

The experimental structures were interpreted with the aid of periodic DFT calculations. When the coordinates obtained at 100 K were optimised with the BLYP functional the root-mean-square deviation of the optimised and experimental non-hydrogen coordinates calculated over a cluster of 15 molecules was 0.087 Å. When a similar procedure was applied to the results of the XN refinement of phase-II at 0.84 GPa the root-mean-square deviation for all atoms was 0.074 Å.

This close agreement is consistent with a recent bench-marking study of the performance of periodic DFT in reproducing molecular crystal structures.[65] Periodic DFT calculations have also been shown to reproduce within 1-2% the unit cell parameters of a variety of simple organic molecular crystal structures.[66] These findings show that structures optimised by DFT can be used as a source of restraints in crystal structure refinements either against powder data or high-pressure single-crystal data suffering from low completeness as a result of shading of reciprocal space by the body of the pressure cell. In many high-pressure structure refinements molecular geometry is restrained to be the same as that in a high-resolution ambient pressure structure determination. Here, the refinements were restrained using structural parameters optimised by periodic DFT which has the advantage that it is not necessary to assume that bond distances and angles are unaffected by pressure. When the DFT-optimised fractional coordinates were applied to the XN refinement as restraints the RMS fit parameters described above changed to 0.065 Å.

The results of a DFT vibrational frequency calculation were used to simulate the inelastic neutron scattering spectrum of aniline-I, and the results are compared with the experimental spectrum[67] in Figure S1 in the supplementary material. The agreement, particularly in the envelope of bands at low frequency, gives us confidence in using such calculations to investigate the thermodynamic properties of aniline under different conditions.

PIXEL calculations yield a total packing energy and a breakdown into component intermolecular interactions. Each interaction energy is further broken down into its Coulombic (electrostatic), polarisation, dispersion and repulsion contributions. These features make such calculations extremely attractive for interpreting crystal packing and investigating the thermodynamic driving forces for phase transitions. Gavezzotti has demonstrated that the PIXEL method can reproduce experimental sublimation enthalpies satisfactorily for 172 organic compounds.[6] The results of PIXEL calculations also compare well with more elaborate quantum

mechanical calculations.[68] For aniline itself, we estimate the sublimation enthalpy to be 67(4) kJ mol^{-1} at 267 K from the following thermodynamic data: $\Delta H_{fus,\ 267K}$ = 10.54(1) kJ mol^{-1}, $\Delta H_{vap,\ 273K}$ = 55(4) kJ mol^{-1}, estimates of the mean C_p heat capacities for the liquid and the vapour between 267 and 273 K are 188 and 107 J mol^{-1}K^{-1} (data taken from http://webbook.nist.gov and ref [69]). A PIXEL calculation based on the DFT-optimised coordinates of aniline at 252 K yielded a lattice energy of 78.8 kJ mol^{-1}. Part of the discrepency between the two estimates of the lattice energy is that the gas-phase geometry differs from that in the solid state in the orientation of the amino group, something not taken into account in the PIXEL calculation. By allowing the geometry of the gas-phase molecule to relax using DFT/BLYP calculations we estimate that the energy of this rearrangement is 3.5 kJ mol^{-1}, giving a combined calculated lattice energy of 75.4 kJ mol^{-1} in good agreement with the experimental value.

Discussion

Hydrogen Bonds

Previous work on the effect of pressure on organic solids has shown that though the lengths of hydrogen bonds are sensitive to pressure, distances are not reduced to beyond the limit for similar contacts in ambient-pressure structures. The lower limit for normalised H…N and N...N contacts in NH…N H-bonds between aromatic amines are 2.03 and 3.04 Å, respectively, in CSD refcode FIDMAH.[70] Details of the search and histograms showing the results are available in Figure S2 in the supplementary material. In aniline-II at 7.3 GPa the H-bonds are substantially shorter than these values, with N11-H112…N12 having an H…N distance of 1.90(4) Å and a N…N distance of 2.85(3) Å, making aniline-II an unusual example where pressure-induced shortening of H-bonds goes beyond the CSD limit. The energies of the H-bonds become similar to those of the CH…π contacts, with N11-H112…N12 pushed into a destabilising region of its potential. This observation illustrates how high pressure can be used to manipulate the hierarchy of energies of intermolecular interactions, making it a potentially powerful tool in crystal engineering.

The Phase II → I Transition Pressure

Aniline-I can be reproducibly grown at ambient pressure by cooling from the liquid. The lack of any further anomaly in heat capacity measurements[69] suggests that this phase remains the thermodynamically stable form down to 2 K. Crystallisation of aniline at 0.8 GPa reproducibly yields phase-II, and above this pressure phase-II is the thermodynamically stable form. A partial transformation from phase-II to phase-I was observed on decompression of phase-II in the powder experiments at 0.35 GPa.

Ultrasonic measurements[21] and decompression of solid aniline indicates that its freezing pressure is around 0.2 GPa, but crystallisation from the liquid phase was never observed below 0.65 GPa. In the neutron powder

experiment a sample of phase-I was obtained by relatively rapid compression of the melt to 0.65 GPa in order to avoid possible loss of fluid at very low loads. This suggests that the transition pressure lies between 0.65 and 0.8 GPa, but the history of the sample makes it possible that seeds of phase-I were present, and the conclusion to be drawn from this observation is less definitive than it might appear.

Though the structures of phases I and II are similar, the reorientation of the molecules which occurs during the transition appears to be reconstructive, and phases I and II can also exhibit metastability. The sample of phase-I grown at 0.65 GPa did not transform to phase-II even at 1.04 GPa, while a single crystal of phase-II did not transform to phase-I on decompression.

All of this makes definition of the exact cross-over point in the stabilities of the two phases rather difficult to define. It lies somewhere between 0.35 and 0.8 GPa, but the results do not enable us to be more precise than this.

Thermodynamic analysis

The difference between the phases is evidently rather subtle, so why should one form be stable at low temperature and the other stable at high pressure?

In this study the structures of both phases I and II were obtained at 0.84 GPa and 0.35 GPa, and this enables modelling of the stabilities of the two phases under both sets of conditions. The relative stability of the two phases is determined by Gibbs free energy, $G = U + PV - TS$, where the symbols have their usual thermodynamic meanings. Hudson and co-workers[71] have emphasised the importance of additionally considering the effect of temperature and zero point energy as corrections to the internal energy U. The various contributing terms were calculated using the results of the DFT total energy and vibrational frequency calculations, and the results summarised in Table 3.

P/GPa	0.35			0.84		
	Phase I	Phase II	Difference	Phase I	Phase II	Difference
U	-755155.12	-755154.96	0.16	-755154.79	-755154.62	0.17
H_{vib}	18.05	18.13	0.08	17.68	17.77	0.09
ZPE	307.12	306.70	-0.42	308.10	307.67	-0.43
TS	36.51	36.63	0.12	34.81	35.06	0.26
pV	27.35	27.46	0.11	62.13	61.85	-0.28
$\Delta G = \Delta U + \Delta H_{vib} + \Delta ZPE - T\Delta S + P\Delta V$			**-0.20**			**-0.71**

Table 3. Contributing terms to the free energy of the phase transformation Aniline-I → Aniline-II at 0.35 and 0.84 GPa. T = 298.15 K in all cases. U is the total internal energy at 0 K. ZPE is the zero point energy and H_{vib} is the thermal contribution to the internal energy arising from population of higher vibrational energy levels with increasing temperature. S = vibrational entropy, P = pressure and V = unit cell volume. Energy units are kJ per mole of aniline molecules. All energy values calculated by periodic DFT using the BLYP functional.

The internal energies (U) are derived from the DFT total energies. The BLYP calculations did not include any correction for dispersion, an important term in molecular crystals, and this contribution was calculated separately using Grimme's method[72] and added to the BLYP total energy. At 0.84 GPa the internal energy term favours phase-I by 0.17 kJ mol^{-1}; PIXEL calculations (based on the same optimised geometry) indicate the same energy ordering with a difference of 0.3 kJ mol^{-1}. Neglecting dispersion in the PIXEL calculations yields a greater energy difference, 1.6 kJ mol^{-1}, which can be compared to a value of 1.0 kJ mol^{-1} obtained from the pure BLYP energies. These results indicate that dispersion interactions are important in stabilising phase-II. We also note the consistency between the DFT and PIXEL calculations.

The entropy, thermal (H_{vib}) and zero point energy contributions to the free energy can be calculated from the vibrational frequencies. The calculations were carried out within the harmonic approximation and only at the gamma point of reciprocal space. The use of these approximations can be justified to some extent by the fact that we are interested in energy differences between two very similar structures rather than absolute values. The frequencies which contribute most to the entropy and thermal energy terms lie at low frequencies. In the region below 200 cm^{-1} the frequencies for phase II are lower than those of phase I and the entropy and vibrational enthalpy terms are therefore slightly numerically larger, by 0.09 and 0.26 kJmol^{-1} at 0.84 GPa. The generally slightly lower frequencies in phase-II also mean than its ZPE is lower than that of phase-I (accounting for 0.43 kJ mol^{1} at 0.84 GPa).

The final pV term reflects the need to fill space efficiently as pressure increases. The slightly lower molecular volume in phase II at 0.84 GPa favours this phase by 0.28 kJmol^{-1}.

Overall it can be seen that phase-II has a very slight free energy advantage (-0.71 kJ mol^{-1}) at 0.84 GPa. The terms which are responsible for this are the entropy and ZPE which favour structures with weaker more deformable interactions, and the pV term, arising from the smaller unit cell volume and more efficient packing of phase-II. As the pressure decreases, the free energy difference between phases I and II approaches zero, and at 0.35 GPa a mixture of phases was observed. The contribution from the PV term changes the most, favouring phase-I at 0.35 GPa because the volume of this phase is now slightly smaller than that of phase-II.

The results presented are the result of making several assumptions and then taking differences between large numbers (Table 3), and they should be viewed as giving insight into the factors governing the stabilities of the two phases under different conditions rather than a definitive statement of free energy differences. This said, they indicate that although aniline-I and II are structurally very similar, the greater compressibility of phase-II lends it higher stability than phase-I at elevated pressures. The pressure x volume term is very important in determining the stability of high pressure phases, becoming ever more important as pressure increases. Although it is usually found to be the dominant factor at high pressure other energy terms can be important. For example, in the transition from salicylaldoxime phase-I to II at 5 GPa,[9] the driving force of the transition was relief of strain built-up in H-bonding and stacking interactions rather than volume reduction. Another

example is provided by salicylamide,[8] in which a high-pressure form grown at 0.2 GPa has entropy as the most important stabilising term.

Conclusions

Two crystalline phases of aniline have been investigated by a combination of single crystal X-ray diffraction data on aniline-h_7 and neutron powder diffraction data on aniline-d_7. Phase I, which is formed on cooling the liquid at ambient pressure is monoclinic ($P2_1/c$) and contains two molecules in the asymmetric unit. Phase-II was crystallised at 0.8 GPa and structurally characterised at pressures up to 7.3 GPa. It is orthorhombic ($Pna2_1$), but with metrically similar unit cell lengths to phase-I; it also has two molecules in the asymmetric unit. Modelling of the high-pressure powder diffraction data was greatly facilitated by incorporating results of DFT geometry optimisations into the refinement in the form of restraints.

In both phases the amino group is displaced by a little over 0.1 Å from the plane of the phenyl group. The amino group is also twisted about the C-N bond, causing the molecule to deviate from C_s symmetry. The structures of the two phases are similar. The strongest interactions are N-H…π contacts which form chains, which are then connected by N-H…N H-bonds. The double chains so formed are linked by π…π and C-H…π contacts into layers. The layers then form stacks mediated by CH…π contacts. The two phases differ in the symmetry relationships which generate the stacks, and the structures only superimpose exactly in every fourth layer.

One of the aims of the work described in this paper was to use high pressure to alter the hierarchy of intermolecular interactions in an organic solid, with NH…N hydrogen bonds being targeted on account of their being relatively weak. The PIXEL method was used to show how the energies of the intermolecular interactions vary with pressure. The NH…π interactions are the most stabilising contacts at all pressures, their energies only changing 5 $kJmol^{-1}$ or less between ambient pressure and 7.3 GPa even though the NH…centroid distance decreases by upwards of 0.3 Å. The NH…N H-bonds are, by contrast, much more sensitive to pressure, in one case changing in energy from -12.8 $kJmol^{-1}$ to +1 $kJmol^{-1}$ for a similar decrease in H…N distance. Energetically, this makes them similar to several of the CH…π contacts. Other CH…π contacts also become destabilising at 7.3 GPa. While the calculation of the dispersion, polarisation and repulsion terms in PIXEL calculations is semi-empirical and potentially approximate particularly in compressed systems, these data indicate that repulsive interactions can be effectively trapped in the compressed lattice.

At room temperature phase II is the thermodynamically stable form above 0.8 GPa. Decompression of this phase yielded a mixture of phases I and II at 0.35 GPa, and phase-I is thermodynamically stable below this pressure and the melting pressure (0.2 GPa). At ambient pressure phase-I is the stable form below 253 K.

Although the structures are very similar, transitions between the two phases are kinetically rather sluggish, making it difficult to pin-point the transition pressure within the range 0.35-0.8 GPa. More positively, this feature has enabled the structures of both phases to be obtained under two sets of identical conditions, at 0.84 GPa and 0.35 GPa, enabling analysis of the thermodynamic properties which govern the stabilities of the two forms under different sets of conditions.

DFT calculations show that phase II is favoured over phase-I at 0.84 GPa by its smaller volume and lower vibrational frequencies, which lead to advantages in entropy and zero point energy. The volume of phase-II becomes larger than that of phase-I at 0.35 GPa; differences in other energy terms either stay the same or diminish, and overall the free energies of phases I and II converge as the pressure is reduced. The relative stability of phase-II with increasing pressure can thus be traced to its greater capacity for packing molecules efficiently.

References

[1] P. T. A. Galek, F. H. Allen, L. Fabian and N. Feeder, *CrystEngComm*, 2009, **11**, 2634-2639.

[2] N. P. Funnell, W. G. Marshall and S. Parsons, *CrystEngComm*, 2011, **13**, 5841-5848.

[3] A. Gavezzotti, *CrystEngComm*, 2003, **5**, 439-446.

[4] A. Gavezzotti, *CrystEngComm*, 2003, **5**, 429-438.

[5] A. Gavezzotti, *Zeitschrift fuer Kristallographie*, 2005, **220**, 499-510.

[6] A. Gavezzotti, *Molecular Aggregation: Structure Analysis and Molecular Simulation of Crystals and Liquids*, Oxford University Press, Oxford, UK, 2007.

[7] R. D. L. Johnstone, D. Francis, A. R. Lennie, W. G. Marshall, S. A. Moggach, S. Parsons, E. Pidcock and J. E. Warren, *CrystEngComm*, 2008, **10**, 1758-1769.

[8] R. D. L. Johnstone, A. R. Lennie, S. F. Parker, S. Parsons, E. Pidcock, P. R. Richardson, J. E. Warren and P. A. Wood, *CrystEngComm*, 2010, **12**, 1065-1078.

[9] P. A. Wood, R. S. Forgan, D. Henderson, S. Parsons, E. Pidcock, P. A. Tasker and J. E. Warren, *Acta Crystallographica, Section B: Structural Science*, 2006, **B62**, 1099-1111.

[10] P. A. Wood, D. Francis, W. G. Marshall, S. A. Moggach, S. Parsons, E. Pidcock and A. L. Rohl, *CrystEngComm*, 2008, **10**, 1154-1166.

[11] P. A. Wood, D. A. Haynes, A. R. Lennie, W. D. S. Motherwell, S. Parsons, E. Pidcock and J. E. Warren, *Crystal Growth & Design*, 2008, **8**, 549-558.

[12] C. A. Morrison and M. M. Siddick, *Chem. Eur. J.* , 2003, **9**, 628-634.

[13] S. Crawford, M. T. Kirchner, D. Blaeser, R. Boese, W. I. F. David, A. Dawson, A. Gehrke, R. M. Ibberson, W. G. Marshall, S. Parsons and O. Yamamuro, *Angewandte Chemie, International Edition*, 2009, **48**, 755-757.

[14] D. R. Allan, W. G. Marshall, D. J. Francis, I. D. H. Oswald, C. R. Pulham and C. Spanswick, *Dalton Transactions*, 2010, **39**, 3736-3743.

[15] F. P. A. Fabbiani, D. R. Allan, A. Dawson, D. J. Francis, W. G. Marshall and C. R. Pulham, *Inorganica Chimica Acta*, 2008, **361**, 487-494.

[16] M. Podsiadlo and A. Katrusiak, *Acta Crystallographica, Section B: Structural Science*, 2006, **B62**, 1071-1077.

[17] M. Yamashita, S. Inomata, K. Ishikawa, T. Kashiwagi, H. Matsuo, S. Sawamura and M. Kato, *Acta Crystallographica, Section E: Structure Reports Online*, 2007, **E63**, o2762-o2764.

[18] I. D. H. Oswald, A. Hamilton, C. Hall, W. G. Marshall, T. J. Prior and C. R. Pulham, *Journal of the American Chemical Society*, 2008, **130**, 17795-17800.

[19] M. Fukuyo, K. Hirotsu and T. Higuchi, *Acta Crystallographica, Section B: Structural Crystallography and Crystal Chemistry*, 1982, **B38**, 640-643.

[20] G. N. R. Tripathi, *Journal of Chemical Physics*, 1980, **73**, 5521-5530.

[21] T. Takagi, *Review of Physical Chemistry of Japan*, 1978, **48**, 10-16.

[22] M. A. Palafox, M. Gill, N. J. Nunez, V. K. Rastogi, L. Mittal and R. Sharma, *International Journal of Quantum Chemistry*, 2005, **103**, 394-421.

[23] P. W. Bridgman, *Physical Review*, 1914, **3**, 153-203.

[24] R. Boese and M. Nussbaumer, *In Situ Crystallisation Techniques*, Oxford University Press, Oxford, UK, 1994.

[25] Bruker-Nonius, *SAINT version 7, Program for integration of area detector data*, 2006.

[26] G. M. Sheldrick, *SADABS Version 2008-1* 2008, University of Göttingen, Germany.

[27] A. Altomare, G. Cascarano, C. Giacovazzo, A. Guagliardi, M. C. Burla, G. Polidori and M. Camalli, *Journal of Applied Crystallography*, 1994, **27**, 435.

[28] P. W. Betteridge, J. R. Carruthers, R. I. Cooper, K. Prout and D. J. Watkin, *Journal of Applied Crystallography*, 2003, **36**, 1487.

[29] R. I. Cooper, R. O. Gould, S. Parsons and D. J. Watkin, *Journal of Applied Crystallography*, 2002, **35**, 168-174.

[30] L. Merrill and W. A. Bassett, *Review of Scientific Instruments*, 1974, **45**, 290-294.

[31] S. A. Moggach, D. R. Allan, S. Parsons and J. E. Warren, *Journal of Applied Crystallography*, 2008, **41**, 249-251.

[32] G. J. Piermarini, S. Block, J. D. Barnett and R. A. Forman, *Journal of Applied Physics*, 1975, **46**, 2774-2780.

[33] Agilent, *Crysalis PRO*, (2010) Crysalis PRO, Agilent Technologies, Yarnton, England.

[34] R. H. Blessing, *Journal of Applied Crystallography*, 1997, **30**, 421-426.

[35] W. G. Marshall and D. J. Francis, *Journal of Applied Crystallography*, 2002, **35**, 122-125.

[36] R. J. Angel, *Journal of Physics: Condensed Matter*, 1993, **5**, L141-L144.

[37] ISIS, ISIS 96-ISIS Facility Annual Report 1995-96, Rutherford Appleton Laboratory, 1996, RAL-TR-96-050, 61-62.

[38] ISIS, ISIS 97-ISIS Facility Annual Report 1996-7, Rutherford Appleton Laboratory, 1997, RAL-TR-97-050, 28-29.

[39] A. Coelho, *TOPAS-Academic: General Profile and Structure Analysis Software for Powder Diffraction Data. Version 5*, 2012.

[40] B. Delley, *Journal of Chemical Physics*, 1990, **92**, 508-517.

[41] Accelrys_Software_Inc, *Materials Studio Release Notes, Release 6.0.0*, (2011), San Diego.

[42] B. Delley, *Journal of Chemical Physics*, 1990, **92**, 508-517.

[43] A. D. Becke, *Journal of Chemical Physics*, 1988, **88**, 2547-2553.

[44] C. Lee, W. Yang and R. G. Parr, *Physical Review B: Condensed Matter and Materials Physics*, 1988, **37**, 785-789.

[45] H. J. Monkhorst and J. D. Pack, *Physical Review B*, 1976, **13**, 5188-5192.

[46] G. M. Sheldrick, *XPREP*, (2001) Bruker-AXS, Madison, WIsconsin, USA.

[47] M. J. Frisch, G. W. Trucks, H. B. Schlegel, G. E. Scuseria, M. A. Robb, J. R. Cheeseman, G. Scalmani, V. Barone, B. Mennucci, G. A. Petersson, H. Nakatsuji, M. Caricato, X. Li, H. P. Hratchian, A. F. Izmaylov, J. Bloino, G. Zheng, J. L. Sonnenberg, M. Hada, M. Ehara, K. Toyota, R. Fukuda, J. Hasegawa, M. Ishida, T. Nakajima, Y. Honda, O. Kitao, H. Nakai, T. Vreven, J. A. Montgomery Jr., J. E. Peralta, F. Ogliaro, M. Bearpark, J. J. Heyd, E. Brothers, K. N. Kudin, V. N. Staroverov, R. Kobayashi, J. Normand, K. Raghavachari, A. Rendell, J. C. Burant, S. S. Iyengar, J. Tomasi, M. Cossi, N. Rega, J. M. Millam, M. Klene, J. E. Knox, J. B. Cross, V. Bakken, C. Adamo, J. Jaramillo, R. Gomperts, R. E. Stratmann, O. Yazyev, A. J. Austin, R. Cammi, C. Pomelli, J. W. Ochterski, R. L. Martin, K. Morokuma, V. G.

Zakrzewski, G. A. Voth, P. Salvador, J. J. Dannenberg, S. Dapprich, A. D. Daniels, Ö. Farkas, J. B. Foresman, J. V. Ortiz, J. Cioslowski and D. J. Fox, *Gaussian 09 , Revision B.01, Gasussian, Inc.*, 2009.

[48] A. Gavezzotti, *OPIX - A computer program package for the calculation of intermolecular interactions and crystal energies*, (2003).

[49] F. H. Allen and W. D. S. Motherwell, *Acta Crystallographica, Section B: Structural Science*, 2002, **58(3, No.1)**, 407-422.

[50] I. J. Bruno, J. C. Cole, P. R. Edgington, M. Kessler, C. F. Macrae, P. McCabe, J. Pearson and R. Taylor, *Acta Crystallographica, Section B: Structural Science*, 2002, **B58(3, No.1)**, 389-397.

[51] C. F. Macrae, I. J. Bruno, J. A. Chisholm, P. R. Edgington, P. McCabe, E. Pidcock, L. Rodriguez-Monge, R. Taylor, J. van de Streek and P. A. Wood, *Journal of Applied Crystallography*, 2008, **41**, 466-470.

[52] K. Brandenburg and H. Putz, *DIAMOND, version 3.2*, (2005) Crystal Impact.

[53] A. J. Ramirez-Cuesta, *Computer Physics Communications*, 2004, **157**, 226–238.

[54] R. J. Angel, *EOSFIT version 5.2*, 2002, Virginia Tech, Blackburg, VA, USA.

[55] A. L. Spek, *Journal of Applied Crystallography*, 2003, **36**, 7-13.

[56] S. K. Wolff, D. J. Grimwood, J. J. McKinnon, M. J. Turner, D. Jayatilaka and M. A. Spackman, *CrystalExplorer (Version 3.0)*, (2012) University of Western Australia, Perth, Australia.

[57] I. J. Bruno, J. C. Cole, M. Kessler, J. Luo, W. D. S. Motherwell, L. H. Purkis, B. R. Smith, R. Taylor, R. I. Cooper, S. E. Harris and A. G. Orpen, *Journal of Chemical Information and Computer Sciences*, 2004, **44**, 2133-2144.

[58] F. H. Allen and I. J. Bruno, *Acta Crystallographica, Section B: Structural Science*, 2010, **B66**, 380-386.

[59] J. J. McKinnon, M. A. Spackman and A. S. Mitchell, *Acta Crystallographica, Section B: Structural Science*, 2004, **B60**, 627-668.

[60] M. A. Spackman and D. Jayatilaka, *CrystEngComm*, 2009, **11**, 19-32.

[61] M. A. Spackman, J. J. McKinnon and D. Jayatilaka, *CrystEngComm*, 2008, **10**, 377-388.

[62] P. Vinet, J. Ferrante, J. H. Rose and J. R. Smith, *J. Geophys Res*, 1987, **92**, 9319-9325.

[63] P. Vinet, J. Ferrante, J. R. Smith and J. H. Rose, *J Phys C: Solid State*, 1986, **19**, L467-L473.

[64] C. Slebodnick, J. Zhao, R. Angel, B. E. Hanson, Y. Song, Z. Liu and R. J. Hemley, *Inorganic Chemistry*, 2004, **43**, 5245-5252.

[65] J. Binns, M. Healey, S. Parsons and C. A. Morrison, *Manuscript in Preparation*, 2012.

[66] B. Civalleri, C. M. Zicovich-Wilson, L. Valenzano and P. Ugliengo, *CrystEngComm*, 2008, **10**, 405-410.

[67] M. H. Herzog-Cance, D. J. Jones, R. El Mejjad, J. Roziere and J. Tomkinson, *Journal of the Chemical Society, Faraday Transactions*, 1992, **88**, 2275-2281.

[68] L. Maschio, B. Civalleri, P. Ugliengo and A. Gavezzotti, *Journal of Physical Chemistry A*, 2011, **115**, 11179-11186.

[69] W. E. Hatton, D. L. Hildenbrand, G. C. Sinke and D. R. Stull, *Journal of Chemical and Engineering Data*, 1962, **7**, 229-231.

[70] V. R. Vangala, R. Mondal, C. K. Broder, J. A. K. Howard and G. R. Desiraju, *Crystal Growth & Design*, 2004, **5**, 99-104.

[71] S. A. Rivera, D. G. Allis and B. S. Hudson, *Crystal Growth & Design*, 2008, **8**, 3905-3907.

[72] S. Grimme, *Journal of Computational Chemistry*, 2006, **27**, 1787-1799.